EurJIC European Journal of Inorganic Chemistry

ChemPubSoc Europe

FULL PAPER

DOI:10.1002/ejic.201301581

Syntheses, Characterization, and Magneto–Structural Analyses in $\mu_{1,3}$-Acetato-Bridged Tetracopper(II) and $\mu_{1,3}$- and $\mu_{1,1,3}$-Acetato-Bridged Pentanickel(II) Clusters

Sudhanshu Das,[a] Lorenzo Sorace,*[b] Averi Guha,[a] Ria Sanyal,[a] Hulya Kara,[c] Andrea Caneschi,[b] Ennio Zangrando,*[d] and Debasis Das*[a]

Dedicated to Professor Marius Andruh on the occasion of his 60th birthday

Keywords: Nickel / Copper / Magnetic properties / Bridging ligands / Cluster compounds

Two pentanuclear Ni^{II} complexes, $[Ni_5(L^1)_2(CH_3COO)_6(OH)_2(MeOH)_2]$ (**1**) and $[Ni_5(L^2)_2(CH_3COO)_6(OH)_2(H_2O)_2]$ (**2**), and one tetranuclear Cu^{II} complex, $[Cu_4(L^3)_2(CH_3COO)_4(O)]$ (**3**), have been synthesized from phenol-based "end-off" compartmental ligands HL^1 to HL^3 {HL^1 = 2,6-bis[ethyl(2-thienyl)iminomethyl]-4-*tert*-butylphenol; HL^2 = 2,6-bis-[ethyl(2-thienyl)iminomethyl]-4-chlorophenol and HL^3 = 2,6-bis[ethyl(2-thienyl)iminomethyl]-4-methylphenol, respectively}. The complexes have been structurally characterized and their magnetic properties have been investigated within the temperature range 2.2–300 K. Complexes **1** and **2** comprise two dinuclear $[Ni_2L^2]$ units linked to a central Ni ion by bridging μ_3-hydroxo groups. The cluster is stabilized by *syn-syn*-$\mu_{1,3}$-bridging and $\mu_{1,1,3}$-bridging acetate anions. The structural analysis of **3** revealed two crystallographically independent complexes that consisted of a tetrahedron of Cu^{II} ions connected to a central μ_4-oxo species and further bridged by four acetate groups along four of the six edges of the Cu_4 core. The other two edges are occupied by μ-phenoxo bridges from the deprotonated L^3 ligand. Magnetic investigations revealed both ferromagnetic and antiferromagnetic interactions in **1** and **2** with single-ion zero-field splitting of magnitude comparable to exchange interactions, and strong antiferromagnetic interactions in **3**.

Introduction

The design and construction of polynuclear transition-metal complexes has been drawing special attention by researchers during the last few decades because of their several intriguing features as well as for their potential applications in the field of magnetism, catalysis, biology, clathration, molecular sieving, and so on.[1–11] In particular, the field of molecular magnetism has seen a large number of these molecules synthesized and characterized in the past decades in the quest for new systems that behave like a single-molecule magnet (SMM).[12] These complexes exhibit interesting phenomena, such as slow magnetization relaxation, magnetization hysteresis, and quantum tunneling of the magnetization (QTM), and they are actively investigated in materials science owing to their potential applications in high-density data storage, molecular spintronics, and quantum computing.[13–16] Among the features required to obtain new SMMs, the most relevant ones are a high-spin ground state and easy axis-type anisotropy,[17] both of which require appropriate design in terms of suitable bridging linkers that mediate magnetic exchange coupling and the coordination environment around metal ions to promote the correct anisotropy.[18] For these reasons, the search for appropriate ligands with a specific geometry to obtain polynuclear complexes of desired nuclearity and with predictable exchange coupling among paramagnetic centers still remains a challenging task for chemists. Incidentally, phenol-based multidentate compartmental ligands turned out to be suitable for synthesizing polynuclear complexes that exhibit interesting magnetic properties.[19–27] It is important to note that compartmental ligands with two adjacent $\{N_2O\}$ donor sets with the phenoxido oxygen atoms available for bridging are often used to prepare a range of homodinuclear complexes.[28–32] However, such ligands can be used also as efficient building blocks to synthesize complexes of higher nuclearity. This can be achieved either (1)

[a] Department of Chemistry, University of Calcutta, 92 A. P. C. Road, Kolkata 700009, India
E-mail: dasdebasis2001@yahoo.com
[b] Dipartimento di Chimica "U. Schiff" and UdR INSTM, Università di Firenze, 50019 Sesto Fiorentino (FI), Italy
[c] Department of Physics, Faculty of Science and Art, Balikesir University, 10145 Balikesir, Turkey
[d] Dipartimento di Scienze Chimiche e Farmaceutiche, University of Trieste, Via L. Giorgieri 1, 34127 Trieste, Italy
Supporting information for this article is available on the WWW under http://dx.doi.org/10.1002/ejic.201301581.

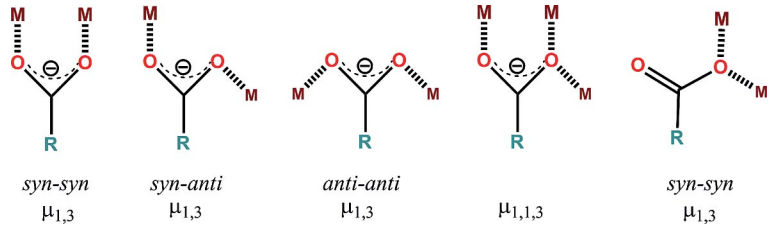

Scheme 1. Different bridging modes of carboxylates.

by properly tuning the reaction condition or (2) by using bridging anions such as carboxylate ($RCOO^-$), azide (N_3^-), and so on. A plethora of polynuclear complexes built with compartmental ligands are available in the literature,[26,33–36] but most of those reports are for copper-based molecules. In contrast, polynuclear nickel complexes of high nuclearity (>3) using similar ligand systems are rather rare, and only three structurally characterized species have been reported in the literature by Fenton and co-workers, who described pentanuclear nickel(II) clusters using tetra- and pentadentate asymmetric dicompartmental ligands with{N_3O} or {N_3OS} donor sets in the presence of acetate anion.[37,38] Owing to diversity in the coordination mode (see Scheme 1) of the carboxylate anion, it can adopt numerous bridging conformations such as *syn-syn*, *syn-anti, anti-anti*, and $\mu_{1,1,3}$ modes,[37–42] and depending on the two binding positions (basal or apical) around the metal ions, these bridging modes can mediate a wide range of exchange interactions. These observations, and by considering the properties shown by carboxylate-containing polynuclear complexes as gas storage,[43–45] molecular recognition,[46,47] molecular magnet,[48–50] catalyst,[51–55] and nonlinear optical materials,[56–58] inspired us to use carboxylate anions in the design of polymetallic species.

In this report we have explored the influence of the carboxylate anion on the structural and magnetic properties of two pentanuclear nickel(II) clusters, namely, $[Ni_5(L^1)_2(CH_3COO)_6(OH)_2(MeOH)_2]$ (**1**) and $[Ni_5(L^2)_2(CH_3COO)_6(OH)_2(H_2O)_2]$ (**2**), and a tetranuclear copper(II) cluster, $[Cu_4(L^3)_2(CH_3COO)_4(O)]$ (**3**), synthesized from phenol-based "end-off" symmetric di-imine compartmental ligands, HL^1 to HL^3 (see Scheme 2). These complexes have been characterized by routine physicochemical techniques and X-ray single-crystal analysis. The variable-temperature magnetic study has shown that both ferromagnetic and antiferromagnetic interactions exist in **1** and **2** and strong antiferromagnetic interactions exist in **3**.

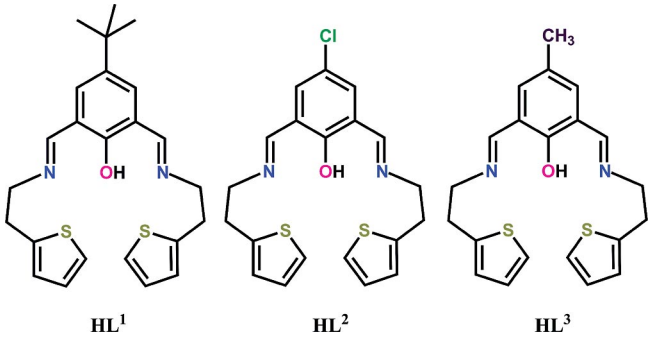

Scheme 2. Phenol-based symmetrical "end-off" compartmental ligands.

Results and Discussion

Synthetic Considerations

2,6-Diformyl-4-methylphenol and 4-*tert*-butyl-2,6-diformylphenol were prepared according to literature methods.[59] The Schiff base ligands HL^1 to HL^3 were prepared by following a reported procedure[60] and their reactions with Ni^{II}–acetate and Cu^{II} have been systematically investigated, as summarized in Scheme 3. When $Ni(CH_3COO)_2\cdot 4H_2O$ was treated with HL^1 and HL^2 in acetonitrile under reflux conditions, complexes **1** and **2**, respectively, were obtained. It is worth mentioning that the use of several Ni/HL^1 or Ni/HL^2 stoichiometric ratios (from 1:1 to 1:4) led only to the pentanuclear complexes for both cases in very high yield. The reaction to prepare **1** is summarized by Equations (1) and (2), whereas the formation of **2** is summarized by Equation (3), which accounts for the formation of hydroxido bridges from water molecules. It is important to note that both reactions are solely controlled by the acetate anion. Use of anions other than acetate do not produce the same result. Detailed studies on the nuclearity dependence on the variation of anions continue in our laboratory. The molar conductivity values (see Table S1 in the Supporting Information) in acetonitrile solvent are consistent with a neutral species, and the elemental analyses are in accord with the formula $[Ni_5(L^1)_2(CH_3COO)_6(OH)_2(MeOH)_2]\cdot 2MeOH$ and $[Ni_5(L^2)_2(CH_3COO)_6(OH)_2(H_2O)_2]\cdot(H_2O)$ for complexes **1** and **2**, respectively, as obtained from the X-ray diffraction analyses. However, no sign of formation of phenoxido-bridged dinuclear species was observed, and invariably a pair of $[Ni_2L^3]$ units sandwiching a central NiO_6 core was obtained, likely on account of greater stability of these species.

However, the reaction of $Cu(CH_3COO)_2\cdot H_2O$ with HL^3 in acetonitrile at room temperature resulted in the formation of complex **3** (Scheme 3). Even in this case, several Cu/HL^3 stoichiometric ratios (from 1:1 to 1:3) were explored, but we failed to prepare a compound of different nuclearity, as the product formation was driven by its higher thermodynamic stability. The formation of **3** is very much controlled by the acetate anion, as is observed in **1** and **2**. It is

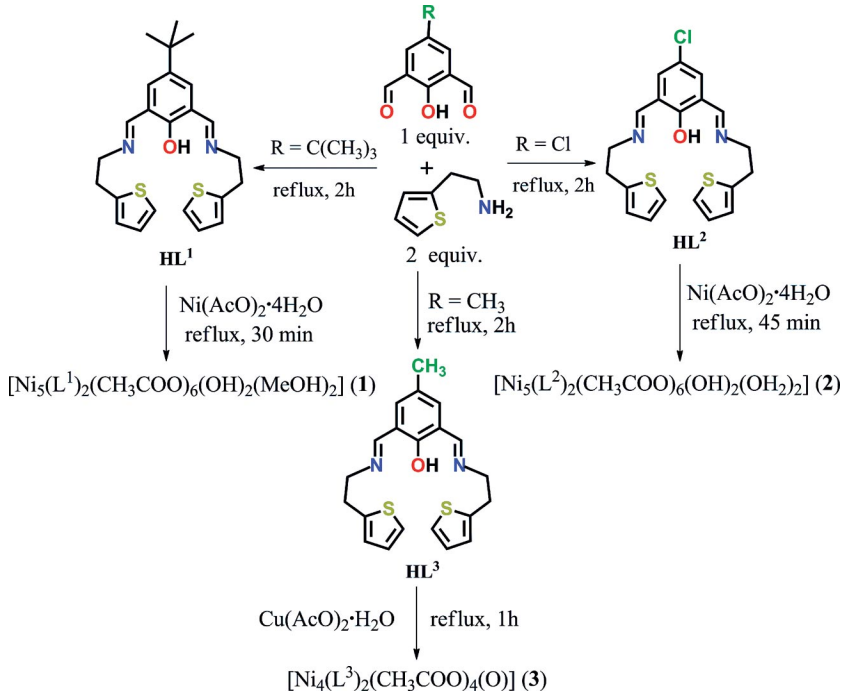

Scheme 3. Reaction scheme.

$$2HL^1 + 5Ni(CH_3COO)_2{\cdot}4H_2O + 2H_2O \rightarrow [Ni_5(L^1)_2(CH_3COO)_6(OH)_2(H_2O)_2] + 4CH_3COOH + 18H_2O \quad (1)$$

$$[Ni_5(L^1)_2(CH_3COO)_6(OH)_2(H_2O)_2] + 4MeOH \rightarrow [Ni_5(L^1)_2(CH_3COO)_6(OH)_2(MeOH)_2]{\cdot}2MeOH \quad (2)$$

$$2HL^2 + 5Ni(CH_3COO)_2{\cdot}4H_2O + 2H_2O \rightarrow [Ni_5(L^2)_2(CH_3COO)_6(OH)_2(H_2O)_2]{\cdot}H_2O + 4CH_3COOH + 17H_2O \quad (3)$$

worth noting that upon dissolution nickel(II) acetate generates a weak acid, acetic acid, and a relatively strong base, nickel(II) hydroxide.[29] As a result, the whole solution becomes weakly basic, a consequence that is supposed to be responsible for generating hydroxy and oxide anions, which in turn act as ligands to make **1**, **2**, and **3**, respectively (see below). The elemental analysis and molar conductivity data are in good agreement with the formula $[Cu_4(L^3)_2(CH_3COO)_4(O)]$, which was confirmed by the X-ray diffraction analysis [Equation (4)].

$$2HL^3 + 4Cu(CH_3COO)_2{\cdot}H_2O + H_2O \rightarrow [Cu_4(L^3)_2(CH_3COO)_4(O)] + 4CH_3COOH + 4H_2O \quad (4)$$

Structural Description of Complexes 1, 2, and 3

The structures of both pentanuclear Ni complexes comprise two dinuclear $[Ni_2L]$ units that are linked to a central Ni ion by bridging μ_3-hydroxo groups. This bridging is augmented by *syn-syn* μ_2-bridging and μ_3-bridging acetate anions so that the central nickel atom is six-coordinate in a distorted-octahedral O_h geometry. All the other nickel atoms have a distorted-octahedral $\{NO_5\}$ chromophore. The coordination bond lengths and angles in both complexes reported in Tables 1 and 2 are comparable in length, and the central Ni ion has coordination bond values comparable to those observed for the metal ions bridged by the phenolato ligands. The detailed structural description is reported below starting with complex **1**, which presents a C_2 symmetry.

Table 1. Coordination bond lengths [Å] and intermetallic distances [Å] for complex **1**.[a]

Ni1–N1	2.023(6)	Ni2–N2	2.049(6)
Ni1–O1	2.018(5)	Ni2–O1	2.022(5)
Ni1–O2	2.007(4)	Ni2–O2	2.025(4)
Ni1–O3	2.121(5)	Ni2–O4	2.073(5)
Ni1–O5	2.034(5)	Ni2–O7	2.124(5)
Ni1–O9	2.269(5)	Ni2–O10#1	2.063(5)
Ni3–O2	2.009(4)	Ni1–Ni2	2.9776(15)
Ni3–O6	2.063(5)	Ni1–Ni3	3.1168(13)
Ni3–O9	2.088(5)	Ni2–Ni3	3.6222(17)
Ni1–O1–Ni2	95.0(2)	Ni1–O2–Ni3	101.81(19)
Ni1–O2–Ni2	95.20(19)	Ni2–O2–Ni3	127.8(2)

[a] Symmetry code: #1 $-x + 1$, y, $-z + 3/2$.

Figure 1 shows the molecular structure of complex **1**. The central metal Ni3 (which sits on a crystallographic twofold axis) has an O_6 donor set, and both Ni1 and Ni2 have a $\{NO_5\}$ donor compartment that, for the former, is provided by the imino-N atom, the bridging phenolato-O atom, the μ_3-OH, and three acetato-O atoms, whereas for Ni2 one acetate O is replaced by a methanol molecule (O7). The metal triangles defined by μ_3-OH are rather distorted, which reflects the nature and connectivity of the bridges: the Ni1···Ni2 distance, fixed by the tridentate phenolato li-

Table 2. Coordination bond lengths [Å] and intermetallic distances [Å] for complex **2**.

Ni1–N1	2.038(7)	Ni3–N3	2.034(7)
Ni1–O1	2.035(5)	Ni3–O8	2.126(5)
Ni1–O2	2.027(5)	Ni3–O11	2.052(5)
Ni1–O3	2.106(5)	Ni3–O12	2.026(5)
Ni1–O5	2.025(6)	Ni3–O13	2.071(5)
Ni1–O9	2.167(5)	Ni3–O3w	2.096(6)
Ni2–N2	2.025(6)	Ni4–N4	2.021(7)
Ni2–O1	2.036(5)	Ni4–O10	2.064(5)
Ni2–O2	2.005(5)	Ni4–O11	2.027(5)
Ni2–O4	2.094(5)	Ni4–O12	2.019(5)
Ni2–O7	2.090(5)	Ni4–O15	2.112(6)
Ni2–O1w	2.102(6)	Ni4–O2w	2.111(7)
Ni5–O2	1.993(5)	Ni1–Ni2	2.9723(14)
Ni5–O6	2.055(6)	Ni1–Ni5	3.1185(14)
Ni5–O8	2.141(5)	Ni2–Ni5	3.5431(14)
Ni5–O9	2.108(5)	Ni3–Ni4	3.0612(14)
Ni5–O12	1.988(5)	Ni3–Ni5	3.1075(13)
Ni5–O14	2.068(6)	Ni4–Ni5	3.5003(14)
Ni1–O1–Ni2	95.05(16)	Ni3–O11–Ni4	94.01(15)
Ni1–O2–Ni2	95.29(15)	Ni3–O12–Ni4	94.59(15)
Ni1–O2–Ni5	102.66(15)	Ni3–O12–Ni5	101.57(16)
Ni2–O2–Ni5	125.85(19)	Ni4–O12–Ni5	128.01(18)

gand and a bridging acetate anion, is 2.9723(14) Å; Ni1···Ni3, which is triply bridged by a *syn-syn* bidentate acetate and a single O from a monodentate acetate beside the capping OH, is 3.1168(13) Å; and the Ni2···Ni3 distance is 3.6222(17) Å, connected by a single bridging acetate only. Figure 2 provides a side view of complex **2** in which the phenolato ligands [which form a dihedral angle of 75.7(1)°] draw a rigid basket-shaped structure that is delineated also by the two μ_3-acetate moieties. Of the lattice methanol molecules, one behaves like a hydrogen donor towards acetate atom O6 [O···O 2.656(9) Å] and like a hydrogen acceptor with respect to the hydroxo O2–H and the coordinated methanol O7 with weaker interactions. The other methanol is appended to O3.

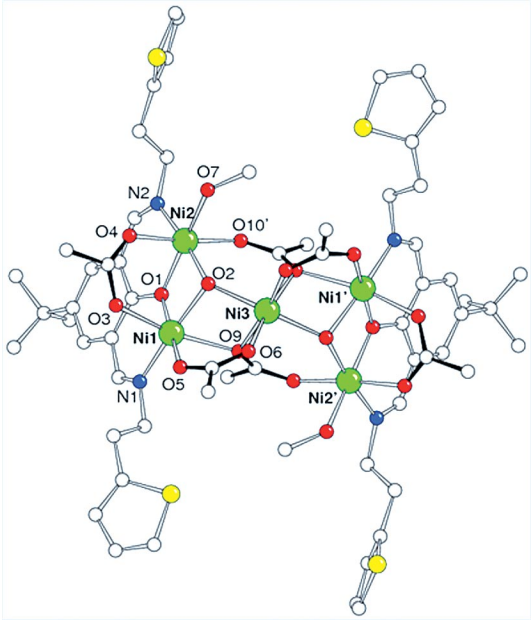

Figure 1. Molecular structure of **1** viewed down the twofold axis with atom labels of crystallographically independent donor atoms.

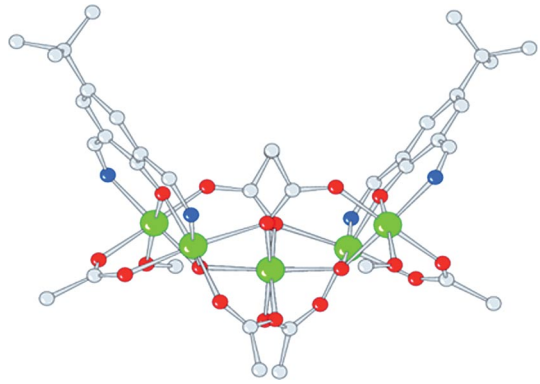

Figure 2. Side view of complex **1** [–$(CH_2)_2$–thienyl chains removed for the sake of clarity]. In this complex, the phenolato ligands [forming a dihedral angle of 75.7(1)°] draw a rigid basket-shaped structure also delineated by the two μ_3-acetate moieties.

Complex **2** presents a pseudo-twofold axis if ethylthienyl chain fragments are excluded, and relative to **1**, the difference in the metal coordination sphere is represented by the substitution of the coordinated methanol molecules by aqua ligands for two of the metals. Figure 3 represents the molecular structure of **2**. The coordination bond lengths reported in Table 2 indicate that values that pertain to the central metal ion (Ni5) are comparable to those observed for the peripheral nickel ions bridged by the phenolato ligands. Again the metal triangles defined by μ_3-OH are scalene. In fact, as noted above for **1**, this reflects the bridging nature and connectivity: the Ni1···Ni2 and Ni3···Ni4 distances bridged by the phenolato are 2.9709(10) and 2.9643(10) Å, whereas Ni1–Ni5 and Ni3–Ni5 are 3.1224(9) and 3.103(1) Å; and finally, Ni2–Ni5 and Ni4–Ni5 are 3.563(1) and 3.606(1) Å, respectively. Figure 4 reports a side

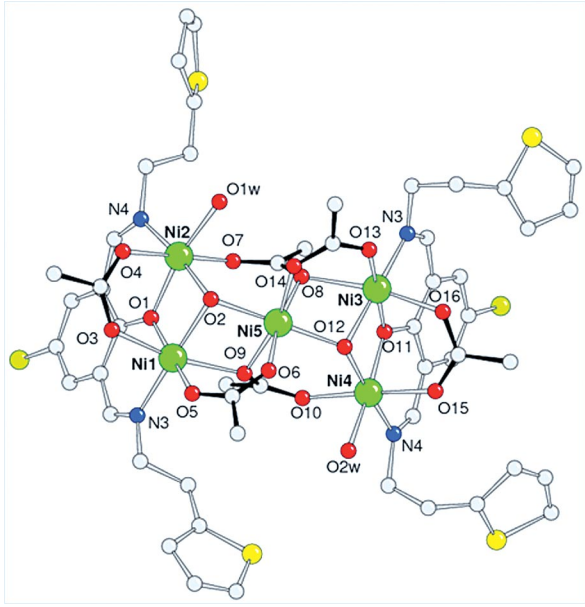

Figure 3. A perspective view of complex **2**.

view of complex **2** that shows the pocket formed by the phenolato ligands, the mean planes of which form a dihedral angle of 80.85(6) to indicate a rigid structure.

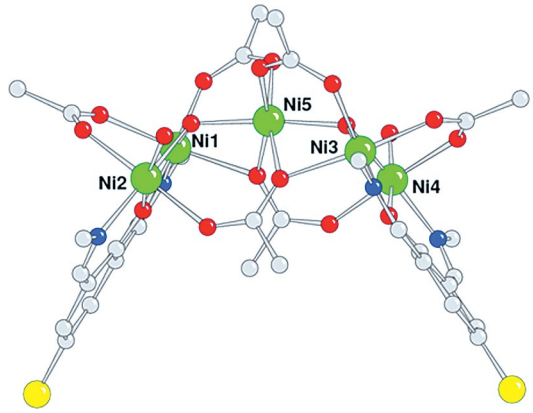

Figure 4. Side view of complex **2** (–CH_2–thienyl fragments are removed for sake of clarity).

The coordinated water O1w and O2w and the lattice molecule O3w form a 1D polymer through a hydrogen-bonding scheme (Figure 5). In particular, the latter has a tetrahedral arrangement that acts as a donor towards acetate oxygen atoms O6 and O13 and as an acceptor with respect to μ_3-hydroxo O12 and water O2w (O···O distance range: 2.74–2.90 Å).

The structural analysis of compound **3** revealed two crystallographically independent complexes that consist of a tetrahedron of copper(II) ions connected to a central μ_4-oxo species and further bridged by four acetate groups along four of the six edges of the Cu_4 core. The other two edges are occupied by μ-phenoxo bridges from the deprotonated L^3 ligand. Figure 6 shows the molecular structure of one of the two crystallographic complexes of **3**. The two complexes show coordination bond lengths and angles (Tables 3 and 4) of comparable values, the main difference being related to the conformational arrangement of the –$(CH_2)_2$–thienyl fragments of the Schiff base ligands. All the metals present a highly distorted square-planar pyramidal coordination with basal bond lengths that fall in a range from 1.910(4) to 1.999(5) Å. In all cases a carboxylate oxygen occupies the apical position at longer distance [2.252(6)–2.359(6) Å]. In the two Cu_2L^3 phenolato moieties, which are oriented almost perpendicular to each other (dihedral angle of ca. 87°), the metals are separated by approximately 3.0 Å, whereas the other Cu–Cu distances are slightly longer [3.140(1)–3.258(1) Å].

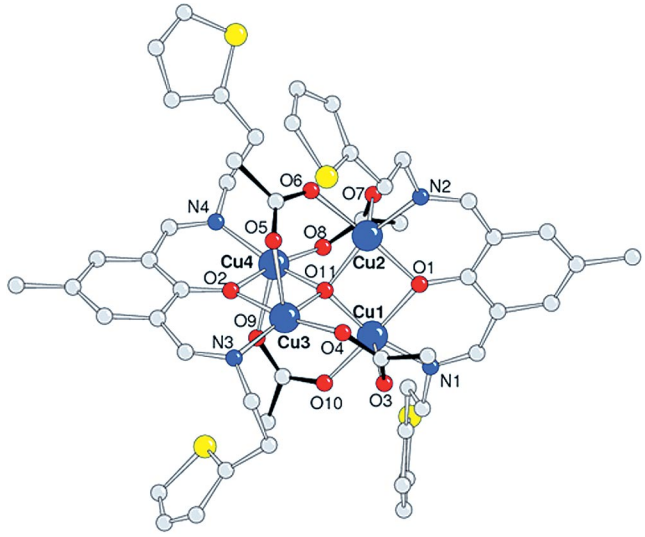

Figure 6. Molecular structure of one of the two crystallographic complexes of **3**.

Magnetic Properties of Complexes 1, 2, and 3

The magnetic properties of complex **1**, in the form of $1/\chi_M$ and $\chi_M T$ (χ_M is the susceptibility per cluster mol) versus T plots, are shown in Figure 7 in the temperature range 2.2–300 K. The magnetic susceptibility conforms well to Curie–Weiss law over the whole investigated range, which gives a negative Weiss constant θ of –1.59 K and a Curie constant of 6.06 emu K mol^{-1}. The θ value suggests the pres-

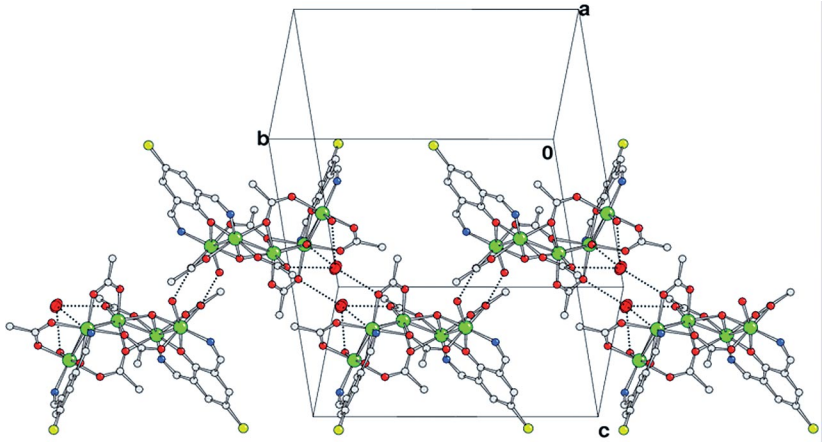

Figure 5. Hydrogen bonds in **2** forming a 1D polymer through aqua O(1w) and O(2w) and the lattice molecule O(3w) (indicated as an ellipsoid).

Table 3. Coordination bond lengths [Å] and intermetallic distances [Å] for complex **3**.

Molecule A		Molecule B	
Cu1–N1	1.986(6)	Cu5–N5	1.971(6)
Cu1–O1	1.999(5)	Cu5–O21	1.988(5)
Cu1–O3	2.353(6)	Cu5–O23	2.289(6)
Cu1–O11	1.910(4)	Cu5–O30	1.952(5)
Cu1–O10	1.932(6)	Cu5–O31	1.919(4)
Cu1–Cu2	3.0069(13)	Cu5–Cu6	3.0046(12)
Cu2–N2	1.976(6)	Cu6–N6	1.962(6)
Cu2–O1	1.977(5)	Cu6–O21	1.959(5)
Cu2–O6	1.937(5)	Cu6–O26	1.942(5)
Cu2–O7	2.354(6)	Cu6–O27	2.359(6)
Cu2–O11	1.915(5)	Cu6–O31	1.921(5)
Cu3–N3	1.954(6)	Cu7–N7	1.994(6)
Cu3–O2	1.969(5)	Cu7–O22	1.970(5)
Cu3–O4	1.942(5)	Cu7–O24	1.920(5)
Cu3–O5	2.337(5)	Cu7–O25	2.359(6)
Cu3–O11	1.920(4)	Cu7–O31	1.922(5)
Cu3–Cu4	2.9951(12)	Cu7–Cu8	3.0085(13)
Cu4–N4	1.980(6)	Cu8–N8	1.987(6)
Cu4–O2	1.958(5)	Cu8–O22	1.993(5)
Cu4–O8	1.962(5)	Cu8–O28	1.946(5)
Cu4–O9	2.252(6)	Cu8–O29	2.297(6)
Cu4–O11	1.920(5)	Cu8–O31	1.912(4)
Cu1–Cu2	3.0069(13)	Cu5–Cu6	3.0046(12)
Cu3–Cu4	2.9951(12)	Cu7–Cu8	3.0085(13)
Cu1–Cu3	3.2582(12)	Cu5–Cu7	3.1956(13)
Cu1–Cu4	3.2113(13)	Cu5–Cu8	3.2174(13)
Cu2–Cu3	3.1401(13)	Cu6–Cu7	3.2103(14)
Cu2–Cu4	3.1483(13)	Cu6–Cu8	3.1538(13)

Table 4. Cu-O-Cu bridging angles [°] for **3**.

Molecule A		Molecule B	
Cu1–O1–Cu2	98.3(2)	Cu5–O21–Cu6	99.1(2)
Cu3–O2–Cu4	99.4(2)	Cu7–O22–Cu8	98.8(2)
Cu1–O11–Cu2	103.7(2)	Cu5–O31–Cu6	103.0(2)
Cu1–O11–Cu3	116.6(2)	Cu5–O31–Cu7	112.6(2)
Cu1–O11–Cu4	113.9(2)	Cu5–O31–Cu8	114.2(2)
Cu2–O11–Cu3	109.9(2)	Cu6–O31–Cu7	113.3(2)
Cu2–O11–Cu4	110.4(2)	Cu6–O31–Cu8	110.7(2)
Cu3–O11–Cu4	102.5(2)	Cu7–O31–Cu8	103.4(2)

ence of a globally weak antiferromagnetic interaction between nickel(II) ions, whereas the Curie constant is in agreement with what is expected for five high-spin Ni^{II} ions, thus indicating a g value of 2.2. The magnetic data were reproduced by using an irreducible tensor operator approach[61] assuming the following spin Hamiltonian [Equation (5)].

$$\hat{H} = -J_1(\mathbf{S_1}\cdot\mathbf{S_2} + \mathbf{S_3}\cdot\mathbf{S_4}) - J_2(\mathbf{S_1}\cdot\mathbf{S_5} + \mathbf{S_3}\cdot\mathbf{S_5}) - J_3(\mathbf{S_2}\cdot\mathbf{S_5} + \mathbf{S_4}\cdot\mathbf{S_5}) + g\beta\mathbf{S}\cdot\mathbf{H} \quad (5)$$

Operators $\mathbf{S_1}$–$\mathbf{S_4}$ represent the peripheral nickel ions (Ni1/Ni2 and N1*/N2*) of the cluster, whereas S_5 represents the central one (Ni3) (Figure 8). The best-fit curve was obtained by using the following values: $g = (2.189 \pm 0.002)$, $J_1 = -(0.62 \pm 0.05)\ cm^{-1}$, $J_2 = -(0.52 \pm 0.4)\ cm^{-1}$, and $J_3 = (-0.52 \pm 0.4)\ cm^{-1}$ (R^2 = 0.0757). However, a very large correlation exists between J_2 and J_3 owing to the symmetry of the Hamiltonian, which does not allow one to discriminate among the interactions between Ni1–Ni3 and Ni2–Ni3 couples despite the structural and coordination differences. Furthermore, use of these values does not provide reasonable agreement with the field-dependent magnetization curve measured at 2.5 K, which would attain a value of 10 Nβ at the highest field versus the experimental one of 7.5 Nβ (see Figure 7, b). We then resorted to a simultaneous fit[62] of both χT versus T and M versus H curve by using a model Hamiltonian with only two coupling constants [Equation (6)].

$$\hat{H} = -J_1(\mathbf{S_1}\cdot\mathbf{S_2} + \mathbf{S_3}\cdot\mathbf{S_4}) - J_2(\mathbf{S_1}\cdot\mathbf{S_5} + \mathbf{S_2}\cdot\mathbf{S_5} + \mathbf{S_3}\cdot\mathbf{S_5} + \mathbf{S_4}\cdot\mathbf{S_5}) \quad (6)$$

In a first step we neglected the contribution of the single-ion zero-field splitting (ZFS) of the five Ni^{II} ions. However, the best-fit parameters obtained by this approach [$J_1 = (0.51 \pm 0.01)\ cm^{-1}$, $J_2 = (-1.14 \pm 0.02)\ cm^{-1}$, g fixed to 2.189] did not provide satisfactory reproduction of the isothermal magnetization curve. This clearly points to non-negligible effects of single-ion ZFS of Ni^{II} on the magnetic properties of this system. Consideration of this term would, however, introduce a large number of additional parameters, namely, the magnitude of the ZFS for the three crys-

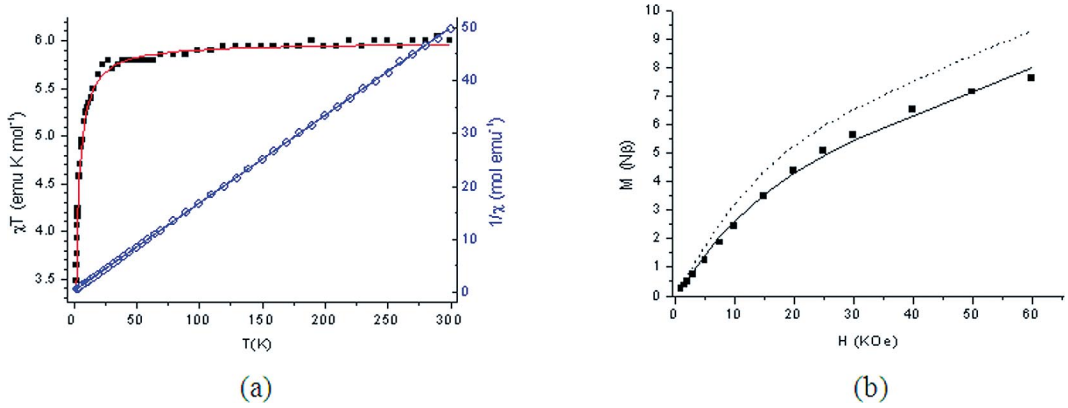

Figure 7. (a) Temperature dependence of $\chi_M T$ and $1/\chi_M$ for complex **1** and best-fit curves obtained using the Hamiltonian model (7) and Curie–Weiss parameters, respectively. Fits obtained using model Hamiltonian (5) and (6) are essentially indistinguishable. (b) Isothermal (T = 2.5 K) field-dependent magnetization for complex **1**, along with best-fit curves obtained by using model Hamiltonian (6) (dotted line), and model Hamiltonian (7) (continuous line), with parameters reported in the text.

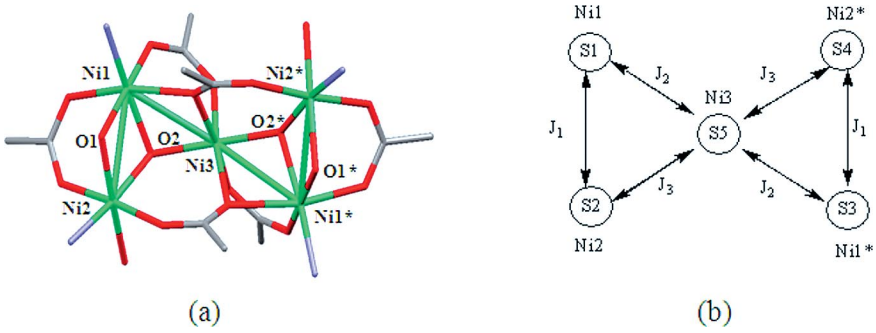

Figure 8. (a) Local coordination environments of Ni^{II} atoms and (b) diagram of the magnetic exchange coupling pathway for complex **1**.

tallographically different Ni^{II} ions and their orientation, which cannot be fixed a priori by symmetry arguments. To reduce over-parametrization, we then considered a model in which the same iso-oriented axial ZFS tensors were assumed for the five Ni^{II} centers, and only the exchange coupling constants were fitted. The Hamiltonian used was then [Equation (7)].

$$\hat{H} = -J_1(\mathbf{S}_1\cdot\mathbf{S}_2 + \mathbf{S}_3\cdot\mathbf{S}_4) - J_2(\mathbf{S}_1\cdot\mathbf{S}_5 + \mathbf{S}_2\cdot\mathbf{S}_5 + \mathbf{S}_3\cdot\mathbf{S}_5 + \mathbf{S}_4\cdot\mathbf{S}_5) + D\sum_{i=1-5}\hat{S}_{zi}^2 \quad (7)$$

Satisfactory reproduction of both curves was obtained by fixing D equal to 4.5 cm^{-1}, which is within the expected range for this type of ion, g_i to 2.189, and J_1 = (1.2 ± 0.1) cm^{-1}, J_2 = (–1.3 ± 0.1) cm^{-1}. Comparison to the fit obtained using Hamiltonian (6) makes it evident that inclusion of ZFS mostly affects the value of J_1, which should then be considered with some caution in view of the assumptions made on the D values.

The magnetic properties of complex **2** are reported in Figure 9 in the forms of $1/\chi_M$ and $\chi_M T$ versus T plots, in the range 1.9–300 K, and as an isothermal magnetization curve at T = 2.5 K. The magnetic susceptibility conforms well to Curie–Weiss law over the whole investigated range to give a negative Weiss constant θ = –2.90 K and a Curie constant of 6.36 emu K mol^{-1}. The θ value suggests the presence of a dominant antiferromagnetic interaction between the nickel(II) ions, whereas the value of the Curie constant is in agreement with what is expected for five high-spin Ni^{II} ions, with $g \approx 2.2$. However, an inspection of the $\chi_M T$ versus T plot immediately shows that, despite the structural similarity with complex **1**, the magnetic behavior is partially different; it does not show the monotonous decrease that characterizes complex **1**. Indeed, upon lowering the temperature, $\chi_M T$ decreases to reach a plateau at 5.3 emu K mol^{-1} between 12 and 8 K then abruptly decreases down to 3.9 emu K mol^{-1} at 1.9 K. The field-dependent magnetization measured at 2 K (Figure 9, b), even if not saturated at 6 T, clearly points to a value somewhat higher than 6 Nβ, which suggests an S = 3 ground state almost exclusively populated at low temperature and high fields. In this framework, the decrease in $\chi_M T$ observed at low temperature has to be attributed to zero-field splitting within the ground state, which can be large owing to the single-ion contribution of Ni^{II} ions.[63] To avoid complications owing to the inclusion of these additional parameters, we first considered data only down to 7 K by using the spin Hamiltonian [Equation (6)] to fit the data.

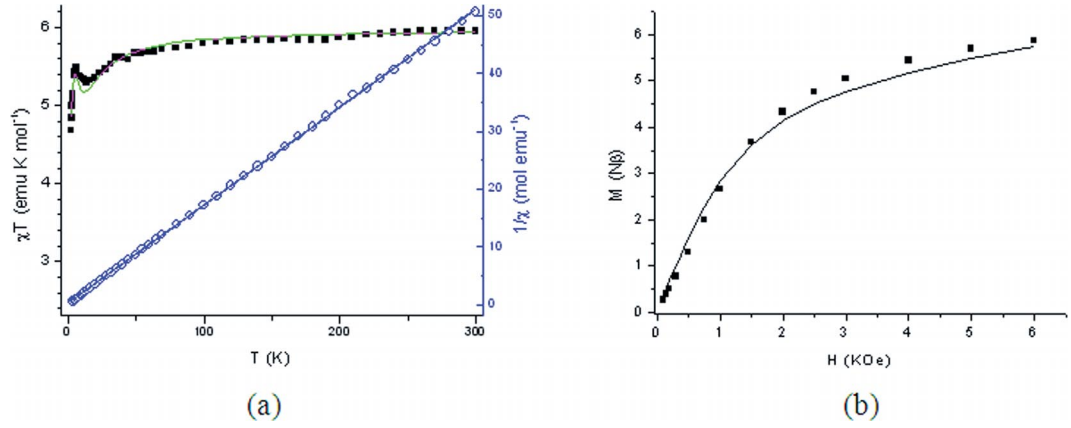

Figure 9. (a) Temperature dependence of $\chi_M T$ and $1/\chi_M$ for complex **2** and best-fit curves obtained using the Hamiltonian model (7) and Curie–Weiss parameters, respectively. (b) Isothermal (T = 2.5 K) field-dependent magnetization for complex **2**, along with best-fit curve obtained by using model Hamiltonian (7) with parameters reported in the text.

The best-fit curve was obtained by using the parameters $g = (2.20 \pm 0.002)$, $J_1 = (4.04 \pm 0.01)\ cm^{-1}$, and $J_2 = (-3.72 \pm 0.01)\ cm^{-1}$. These indeed provide an $S = 3$ ground state with the first $S = 2$ and $S = 1$ excited states at 3.72 and 7.44 cm^{-1}, respectively, thus being in qualitative agreement with the outcome of isothermal magnetization measurements. Field-dependent magnetization data and the full temperature dependence of the χT product could, however, be simultaneously fit only within the same framework of complex **1** (i.e., by considering the same axial iso-oriented ZFS tensor for the five Ni^{II} ions). With this approach, the best-fit curve was obtained by fixing g_i to 2.188 and $J_1 = (4.6 \pm 0.1)\ cm^{-1}$, $J_2 = (-3.8 \pm 0.1)\ cm^{-1}$, and fixing D to 7.5 cm^{-1}.

The combined results of the fits for **1** and **2**, despite the approximations used, clearly indicate that J_1 is ferromagnetic and J_2 is antiferromagnetic; furthermore, for both coupling constants, the magnitude appears to be somewhat larger in **2** than in **1**.

The magnetic properties of complex **3** are shown in Figure 10a in the forms of $1/\chi_M$ and $\chi_M T$ versus T plots in the range 2–300 K. The Curie–Weiss plot of $1/\chi_M$ versus T is not linear, even in the high-temperature regime. The value of $\chi_M T$ at room temperature (1.32 $cm^3\,mol^{-1}\,K$, 3.25 BM) is lower than expected for four uncoupled $S = 1/2$ ions with $g = 2$. (1.5 $cm^3\,mol^{-1}\,K$, 3.46 BM), thus indicating the existence of medium to strong antiferromagnetic superexchange interactions between the copper(II) ions. This is confirmed by the continuous decrease in the $\chi_M T$ product upon decreasing temperature, which reaches a value of 0.0161 $cm^3\,mol^{-1}\,K$ at 2 K that is indicative of an $S = 0$ spin ground state with residual paramagnetism owing to unavoidable impurities. This is confirmed by the field-dependent magnetization data, the very low values of which are in agreement with a diamagnetic ground state and a small fraction of paramagnetic impurities (Figure 10, b), estimated to be about 2%.

As reported in the structural characterization of **3**, there are two crystallographically (and magnetically) independent clusters, A and B, which have the same pattern and similar structural parameters (Figure 11, Tables 3 and 4). In both of them, two different magnetic exchange pathways can be defined in principle: the first one involves the pairs Cu1/Cu2 or Cu3/Cu4, which are bridged by the O1/O2 atom of the phenoxo ligand and by the central μ_4-O11 atom. The second path defines the exchange interaction between Cu1/Cu3, Cu1/Cu4, Cu2/Cu3, and Cu2/Cu4, which are bridged by the central μ_4-O11 atom and carboxylate group. It has to be noted that for the latter four couples, the Cu–O–Cu angles at μ_4-O11 are in the range of 110–116°, whereas the interaction with the carboxylato ligand involves the axial position on one Cu^{II} and a basal position on the other one.

Under this approach, the magnetic properties of **3** should be analyzed by means of the following spin Hamiltonian [Equation (8)].

$$\hat{H} = -J_1(\mathbf{S_1}\cdot\mathbf{S_2} + \mathbf{S_3}\cdot\mathbf{S_4}) - J_2(\mathbf{S_1}\cdot\mathbf{S_3} + \mathbf{S_1}\cdot\mathbf{S_4} + \mathbf{S_2}\cdot\mathbf{S_3} + \mathbf{S_2}\cdot\mathbf{S_4}) \quad (8)$$

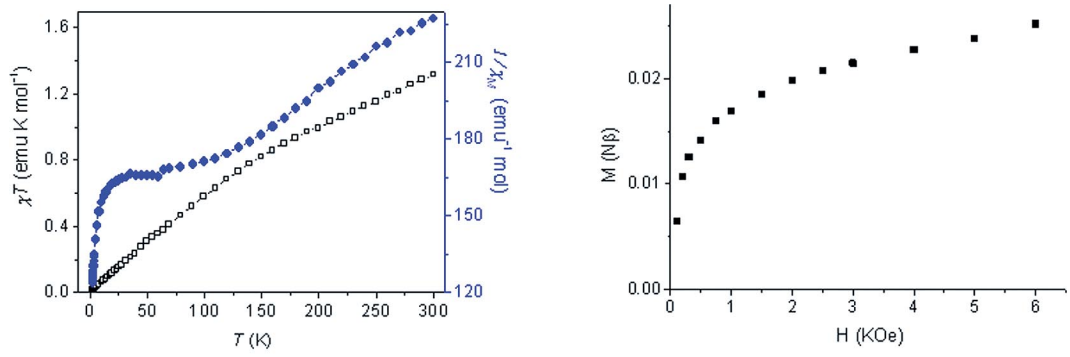

Figure 10. (a) Temperature dependence of $\chi_M T$ and $1/\chi_M$ for **3**. (b) Magnetization as a function of the applied magnetic field for **3**, measured at 2 K.

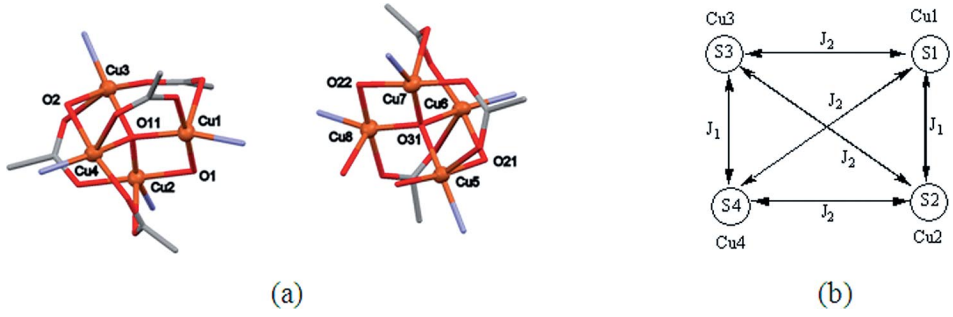

Figure 11. (a) Local coordination environments of Cu^{II} atoms and (b) diagram of the magnetic exchange coupling pathway for complex **3**.

The resulting expression for the magnetic susceptibility is, however, not suitable for a meaningful fit of the data, since the two coupling constants turned out to be highly correlated. Such a problem has already been reported for systems of similar magnetic topology and has partially been solved in the regime of strong antiferromagnetic coupling by using a Bleaney–Bowers equation[64] to reproduce the magnetic properties that arise essentially from the $S = 0$ and the first $S = 1$ excited state. However, this method does not seem appropriate here, since the strong coupling regime is not achieved and other states are possibly populated. As a further complication, one has to note that the coupling constants for the two independent clusters may be, at least partially, different, definitely requiring too many parameters to be fit to a single equation.

Magneto–Structural Correlations

We have examined the magneto–structural correlation on a few pentanuclear nickel(II) and tetranuclear copper(II) complexes published in recent years, and the results are reported in Tables 5 and 6, respectively. The exchange coupling constants obtained for both **1** and **2** are essentially in agreement with expectations; in particular, the ferromagnetic character of J_1 is consistent with the reported magneto–structural correlations in phenoxo-bridged nickel(II) complexes (with θ angles = 90–95°) that contain *syn-syn*-carboxylate and either alkoxo, hydroxo, or water[65,66] bridging ligands (Figure 12, Table 5). We note here that this behavior is due to two different contributions: the ferromagnetic one of the small angle Ni–$O_{phenoxo}$–Ni path, and the carboxylate bridge, which is almost perfectly orthogonal to the Ni_2O_2 plane (89.8°). Some recent theoretical results indicate that the *syn-syn* bridging carboxylate ligand that connects two Ni^{II} ions in triply mixed-bridged complexes shows in some cases an antiferromagnetic contribution to the exchange coupling[67] and in other cases a ferromagnetic contribution.[68] Finally, we note that other structural factors such as the folding of the bridging fragment and the shift of the phenolic carbon atom from the Ni_2O_2 plane have a significant influence on the magnetic coupling in diphenoxo-bridged Ni^{II} complexes. As for J_2, the large Ni1/2–O–Ni3 angle would suggest a relevant value of the antiferromagnetic coupling constant,[65,69] quite in contrast with the experimental findings. However, even in this case, the compensating effect of additional exchange coupling

Table 5. J as a function of the Ni–O–Ni angles and Ni–Ni distances inside the $[Ni_5(\mu_3\text{-}OH)_2]$ core.

Complex[a]	Carboxylate bridging mode	Ni–O–Ni[b] angle [°]	Ni–Ni[c] distance [Å]	J [cm^{-1}]	g	Ref.
$[Ni^{II}_5L^N_4(\mu_3\text{-}OH)_2(\mu_2\text{-}OH_2)_2(EtOH)_2]$	–	95.42–103.88	3.049–3.181	+6.5	2.32	[66]
$[Ni_5(OH)_2(L\text{-}aba)_4(OAc)_4]\cdot 0.4EtOH\cdot 0.3H_2O$	μ_2 and μ_3	94.0–126.9	2.85–3.47	$J_1 = +3.0$, $J_2 = -1.0$	2.08	[65]
$[Ni_5(L_5)_2(OAc)_6(OH)_2]$	μ_2 and μ_3	93.91–95.12	2.986–2.988	–	–	[37]
$[Ni_5(L^1)_2(Ac)_6(OH)_2(MeOH)_2]\cdot 4MeOH$ (**1**)	μ_2 and μ_3	94.96	2.978	very weak, AF	2.189	this work
$[Ni_5(L^2)_2(Ac)_6(OH)_2(H_2O)_2]\cdot(H_2O)$ (**2**)	μ_2 and μ_3	93.99–95.04	2.964–2.971	very weak, AF	2.236	this work

[a] H_2L^N is methylamino-*N*,*N*-bis(2-methylene-4,6-dimethylphenol); L-abaH = L-2-aminobutyric acid; HL_5 = 2-{[(2-dimethylaminoethyl)-ethylamino]methyl}-6-ethyliminomethyl-4-methylphenol. [b] Ni–O–Ni angles only in phenoxide-bridged Ni_2O_2 core. [c] Adjacent Ni–Ni distances in phenoxide-bridged Ni_2O_2 core. S_T = ground-state spin, AF = antiferromagnetic.

Table 6. *J*, Cu–Cu distances [Å], and Cu–O–Cu angles [°] in complexes with $[Cu_4O]$ complex core.

Complex[a]	Carboxylate bridging mode	Cu–O–Cu[b] angle [°]	Cu–Cu[c] distance [Å]	J [cm^{-1}]	S_T	g	Ref.
$[Cu_4(L)_2(O)(OH)_2(MeOH)_2(ClO_4)_2]$	–	100.01–101.25	2.993	–720	0	2.19	[33]
$[Cu_4(O)(L1)_2(CH_3COO)_4]$	*syn-syn*, μ_2	99.56–103.62	3.017	–210			
$[Cu_4(O)(L2)_2(CH_3COO)_4]$	*syn-syn*, μ_2	97.60–101.84	2.977–2.984	–219			
$[Cu_4(O)(L3)_2(CH_3COO)_4]$	*syn-syn*, μ_2	98.44–103.45	2.998–3.010	–227	0,1	–	[34]
$[Cu_4(O)(L4)_2(CH_3COO)_4]$	*syn-syn*, μ_2	97.81–102.39	2.992–2.987	–271			
$[Cu_4(\mu_4\text{-}OH)(dmae)_4][Ag(NO_3)_4]$	–	101.0	2.9472–4.152	$J = +1.8$, $J' = -29.2$	0	2.10	
$[Cu_4(\mu_4\text{-}OH)(dmae)_4][Na(NO_3)_4]$	–	100.7	2.9485–4.149	$J = +2.9$, $J' = -32.2$		2.10	[72]
$[Cu_4(\mu_4\text{-}O)(\mu\text{-}bip)_2(\mu\text{-}O_2CPh)_4]\cdot 0.5CH_2Cl_2$	*syn-syn*, μ_2	101.88–103.74	3.068	–289	0	2.0	
$[Cu_4(\mu_3\text{-}OH)_2(\mu\text{-}bip)_2(N_3)_4]$	–	97.28–102.83	2.986–2.996	–464		2.2	[74]
$[Cu_4\text{-}(\mu_3\text{-}OH)_2(\mu\text{-}bip)_2(NCS)_4(dmf)_2]$	–	100.65–104.38	3.043	–405		2.2	
$[Cu^{II}_4(\mu_3\text{-}L^1)_2(\mu\text{-}OH)_2(H_2O)_2](ClO_4)_2\cdot H_2O$	–	91.98–106.41	3.092–3.095	–16.9	0	2.03	[26]
$[Cu_4(\mu_4\text{-}O)\text{-}(\mu\text{-}cip)_2(\mu_{1,3}\text{-}O_2CPh)_4]\cdot 2CH_3OH$	*syn-syn*, μ_2	99.20–103.39	2.993–3.011	–340	1/2	2.03	[35]
$[Cu^{II}_4(bdmmp)_2(\mu_4\text{-}O)(O_2CCF_3)]$	*syn-syn*, μ_2	98.4–99.1	2.930–2.933	–60	0	2.22	[36]
$[Cu_4(L^3)_2(CH_3COO)_4(O)]$ (**3**)	*syn-syn*, μ_2	98.29–99.41	2.995–3.008	strong, AF	0	2.0	this work

[a] HL = 2,6-bis(pyrrolidinomethyl)-4-methylphenol; HL1 = 4-methyl-2,6-bis(cyclohexylmethyliminomethyl)phenol; HL2 = 4-methyl-2,6-bis(phenylmethyliminomethyl)phenol; HL3 = 4-methyl-2,6-bis{[(3-trifluoromethyl)phenyl]methyliminomethyl}phenol; HL4 = 4-methyl-2,6-bis{[(4-trifluoromethyl)phenyl]methyliminomethyl}phenol; Hdmae = dimethylaminoethanol, Hbip = 2,6-bis(benzyliminomethyl)-4-methylphenol; H_2L^1 = 2-hydroxobenzylidene-[2-(4-{2-[(2-hydroxobenzylidene)amino]ethyl}-piperazin-1-yl)ethyl]amine; Hcip = 2,6-bis(cyclohexyliminomethylene)-4-methylphenol; bdmmpH = 2,6-bis[(dimethylamino)methyl]-4-methylphenol. [b] Cu–O–Cu angles only in phenoxide-bridged Cu_2O_2 core. [c] Adjacent Cu–Cu distances in phenoxide-bridged Cu_2O_2 core. S_T = ground-state spin, AF = antiferromagnetic.

paths[63] has to be considered, and indeed, the values observed in **1** and **2** are consistent with a recent report on an amino acid based pentanuclear nickel cluster.

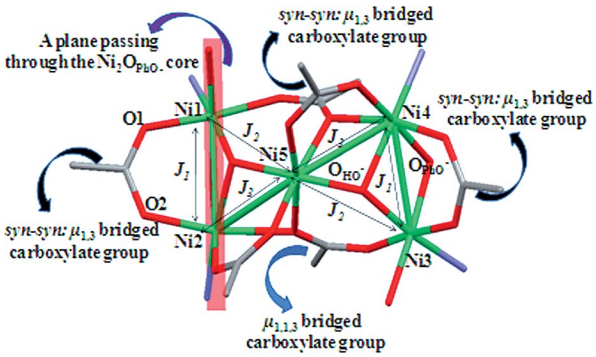

Figure 12. Coordination environment in the [Ni_5] core of complexes **1** and **2** showing the different carboxylate bridging modes.

As for the magnetic behavior of complex **3**, the observation of a relatively strong, albeit not quantitatively determined, antiferromagnetic-type exchange interaction is in good agreement with previously reported data for similar systems.[33,34,70–72] A comparable structural motif is present in $[Cu_4(L^n)_2(O)(O_2CPh)_4]$[70] and $[Cu_4(O)(L^n)_2(Ac)_4]$[34] (L^n = N_2O-donor Schiff base ligand), in which a strong antiferromagnetic exchange coupling of –289(4) cm^{-1} was measured in the former, and in the range from –210.1 to –271.3 cm^{-1} in the second. To understand the antiferromagnetic behavior in this kind of system, it is necessary to consider that two types of exchange interactions, one through μ_2-phenoxido and the other through the *syn-syn*-carboxylato bridge, are active. It is well established that the *syn-syn* bridging mode of the carboxylate ligand causes antiferromagnetic coupling, whereas the μ_2-phenoxido bridge can transmit either antiferro- or ferromagnetic interaction depending on the Cu–O(phenoxido)–Cu bridging angles[71,73] (Table 6). Krebs and co-workers previously reported the temperature-dependent magnetic properties of μ_4-oxo-bridged tetracopper(II) systems, which revealed the antiferromagnetic type of interaction between the copper(II) ions.[33] Ray and co-workers also reported tetracopper(II) complexes with both μ_4-oxo and $\mu_{1,3}$-acetato bridges and studied their magnetic properties extensively, wherein again the interactions between copper(II) centers were found to have an antiferromagnetic nature.[26,35,36,74] In our case, the observed relatively strong antiferromagnetic interaction in complex **3** is very much expected considering the higher Cu–O(phenoxido)–Cu bridging angles (>95°) and is in good agreement with the above reports.

Conclusion

The complexation of Cu^{II} and Ni^{II} acetates with phenol-based symmetrical Schiff base compartmental ligands yielded tetranuclear copper and pentanuclear nickel irrespective of whether the ratio of metal to salt and ligands are maintained. The noncoordinating behavior of the S atom of the thiophene moiety of the end-off compartmental ligands and the bridging property of acetato ligand are supposed to be responsible for generating polynuclear transition-metal assemblies. Variable-temperature magnetic studies in the range 2.2–300 K have shown a dominant antiferromagnetic interaction quite generally for a *syn-syn*-phenoxido and *syn-syn*-carboxylato-bridged tetracopper(II) species. However, pentanuclear nickel complexes have shown weak ferromagnetic interactions owing to the small Ni–O_{PhO}–Ni phenoxo bridging angles close to 90–95° and of *syn-syn*-$\mu_{1,3}$-carboxylato bridge, which is practically orthogonal to the Ni_2O_2 plane. This provides an additional and compensating exchange coupling path. A comparative study of the magnetic properties of **1** and **2** revealed a slight increase in the magnitude of the exchange coupling constants J_1 and J_2 in complex **2**.

Experimental Section

Reagents and Materials: Copper acetate monohydrate and nickel acetate tetrahydrate were purchased from Merck (India). [2-(2-Thiophenyl)ethyl]amine was purchased from Sigma–Aldrich and used without purification. All other chemicals and solvents were of reagent grade and were used as received without further purification.

Synthesis of Ligands HL^1 to HL^3: See Scheme 4; 4-*tert*-butyl-2,6-diformylphenol (0.206 g, 1 mmol) and [2-(2-thiophenyl)ethyl]amine (0.254 g, 2 mmol) were used at a 1:2 equiv. ratio in acetonitrile (15 mL) in a round-bottomed flux and heated under reflux conditions for 2 h as previously reported.[60] A yellow solution of HL^1 was obtained. The solvent was evaporated and an orangelike sticky liquid resulted. The other two ligands, HL^1 and HL^2, were prepared by following the same procedure by using 4-chloro-2,6-diformylphenol (0.189 g, 1 mmol) and 2,6-diformyl-4-methylphenol (0.164 g, 1 mmol), respectively, instead of 2,6-diformyl-4-*tert*-butylphenol. ^{1}H NMR ([D_6]DMSO, 25 °C): For HL^1: δ = 8.589 (s, 2 H, H^c), 7.721 (s, 2 H, H^b), 7.305, 7.290 (d, 2 H, H^f), 6.930 to 6.862

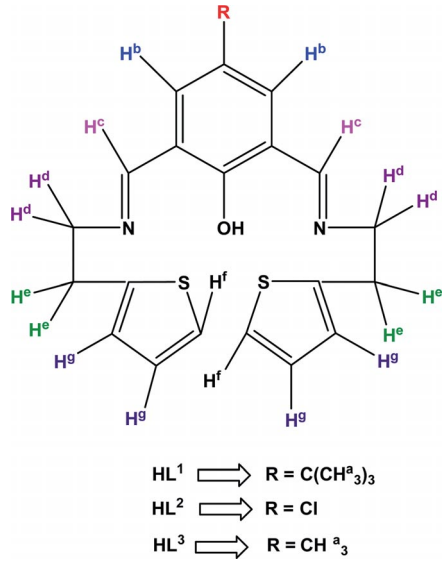

Scheme 4. Structure of the ligands (HL^1–HL^3) with hydrogen labeling.

(m, 4 H, H^g), 3.852, 3.822, 3.800 (t, 4 H, H^d), 3.193, 3.158, 3.135 (t, 4 H, H^e), 1.259 (s, 9 H, H^a) ppm; for HL^2: δ = 8.498 (s, 2 H, H^c), 7.464 (s, 2 H, H^b), 7.281, 7.277 (d, 2 H, H^f), 6.909 to 6.848 (m, 4 H, H^g), 3.814, 3.792, 3.770 (t, 4 H, H^d), 3.145, 3.123, 3.101 (t, 4 H, H^e), 2.204 (s, 3 H, H^a) ppm; for HL^3: δ = 8.690 (s, 2 H, H^c), 7.536 (s, 2 H, H^b), 7.416, 7.411 (d, 2 H, H^f), 6.998 to 6.958 (m, 4 H, H^g), 3.163, 3.148, 3.137 (t, 4 H, H^e), 3.132 (s, 4 H, H^d), 2.226 (s, 3 H, H^a) ppm.

$[Ni_5(L^1)_2(CH_3COO)_6(OH)_2(MeOH)_2]\cdot 2MeOH$ (1): Nickel(II) acetate tetrahydrate (0.620 g, 2.5 mmol) dissolved in water/acetonitrile (10 mL, 1:4 ratio v/v) was added to the yellow solution of HL^1 in acetonitrile (15 mL). Upon stirring the brown solution that had formed initially changed to green within 5–10 min. The green mixture was then heated under reflux conditions for another 1 h to obtain a clear intense green solution. The solution was kept in a dark place. A few days later a powdered solid was obtained. Needle-shaped, green single crystals suitable for X-ray analyses were separated out after recrystallization from methanol, yield 89%. $C_{66}H_{98}N_4Ni_5O_{22}S_4$ (1721.30): calcd. C 46.01, H 5.69, N 3.25; found C 45.88, H 5.56, N 3.17.

$[Ni_5(L^2)_2(CH_3COO)_6(OH)_2(H_2O)_2]\cdot(H_2O)$ (2): Complex **2** was synthesized by adopting a procedure similar to that for complex **1**. Nickel(II) acetate tetrahydrate (0.620 g, 2.5 mmol) dissolved in water/acetonitrile (10 mL, 1:4 ratio v/v) was added to the yellow solution of HL^2 in acetonitrile (15 mL). Upon stirring, the brown solution that had formed initially changed to green in about 10 min. The green mixture was then heated under reflux conditions for 45 min to obtain a very deep green solution. Block-shaped, intense-green single crystals suitable for X-ray analyses were obtained after 2–3 d, yield 82%. $C_{52}H_{62}Cl_2N_4Ni_5O_{19}S_4$ (1539.77): calcd. C 40.56, H 4.06, N 3.64; found C 40.18, H 3.96, N 3.55.

$[Cu_4(L^3)_2(CH_3COO)_4(O)]$ (3): Solid copper(II) acetate monohydrate (0.399 g, 2 mmol) was added dropwise to a yellow solution of HL^3 (0.382 g, 1 mmol) in acetonitrile (25 mL). The resulting solution was heated under reflux conditions for 30–40 min and cooled to room temperature. Crystals suitable for X-ray structural determination formed in the solution, yield 79%. $C_{50}H_{54}Cu_4N_4O_{11}S_4$ (1269.42): calcd. C 47.31, H 4.29, N 4.41; found C 47.01, H 4.17, N 4.32.

Physical Measurements: Elemental analyses (C, H, and N) were performed using a Perkin–Elmer 240C elemental analyzer. FTIR spectra were recorded with a Shimadzu FTIR 8400S instrument with KBr pellets in the 4000–400 cm^{-1} range. The molar conductivity of the synthesized complexes was measured with a Systronics Conductivity Meter 306. Electronic spectra (800–200 nm) in solution were recorded with a Shimadzu UV-3101PC UV/Vis/near-IR spectrophotometer at 28 °C using acetonitrile as medium, whereas those in the solid state were recorded with a Hitachi U-3501 spectrophotometer. DC magnetic measurements were performed with a Cryogenics Squid S600 magnetometer with an applied field of 0.1 T. To avoid possible orientation effects, microcrystalline powders were pressed in pellets. The data were corrected for sample holder contribution, measured in the same field and temperature range (2.2–300 K), and the intrinsic diamagnetism of the sample was measured by using Pascal constants.

Crystallographic Refinement and Structure Solution: Data collections for crystal structure analysis for all complexes were carried out at room temperature with a Bruker Smart Apex diffractometer equipped with charge-coupled device (CCD) and Mo-K_α radiation (λ = 0.71073 Å). Cell refinement, indexing, and scaling of the data sets were carried out with Bruker Smart Apex and Bruker Saint packages.[75] Structures were solved by direct methods and subsequent Fourier analyses[76] and refined by the full-matrix least-squares method based on F^2 with all observed reflections.[77] Owing to their conformational freedom some of the thiophene rings were found disordered: only one of the rings in **2** was successfully refined over two positions at half occupancy (S2/S2a). In other cases, residuals around these groups (difficult to model) indicate a disorder over two coplanar orientations of the thienyl rings, which were refined with restraints on thermal U factors (the ISOR instruction in

Table 7. Crystallographic data and details of refinement for complexes **1**, **2**, and **3**.

	1·2MeOH	**2**·H_2O	**3**
Empirical formula	$C_{66}H_{98}N_4Ni_5O_{22}S_4$	$C_{52}H_{62}Cl_2N_4Ni_5O_{19}S_4$	$C_{50}H_{54}Cu_4N_4O_{11}S_4$
M_r	1721.27	1539.75	1269.37
Crystal system	monoclinic	triclinic	triclinic
Space group	$C2/c$	$P\bar{1}$	$P\bar{1}$
a [Å]	29.618(10)	14.7008(5)	17.988(2)
b [Å]	15.614(4)	16.0701(10)	18.467(2)
c [Å]	18.653(8)	16.4301(6)	18.826(2)
α [°]	–	99.3040(10)	80.742(2)
β [°]	114.174(9)	114.3660(10)	62.9590(10)
γ [°]	–	100.3590(10)	87.158(2)
V [Å^3]	7870(5)	3355.5(3)	5495.7(11)
Z	4	2	4
D_{calcd} [g cm^{-3}]	1.453	1.524	1.534
μ(Mo-K_α) [mm^{-1}]	1.352	1.649	1.739
F(000)	3608	1584	2600
θ range [°]	1.51–24.17	1.34–25.52	1.12–24.57
Reflections collected	14167	39354	37857
Independent reflections	5370	12260	18210
R_{int}	0.1118	0.0343	0.0583
Number of reflections [$I > 2\sigma(I)$]	3423	9636	9294
Refined parameters	459	796	1297
GoF (F^2)	1.054	1.024	1.027
$R1$, $wR2$ [$I > 2\sigma(I)$][a]	0.0609, 0.1570	0.0597, 0.1757	0.0700, 0.1838
Residuals [e Å^3]	0.789, –0.521	1.012, –1.338	1.200, –1.011

[a] $R_1 = \Sigma||F_o| - |F_c||/\Sigma|F_o|$, $wR_2 = [\Sigma w(F_o^2 - F_c^2)^2/\Sigma w(F_o^2)^2]^{1/2}$.

the SHELX refinement program). The ΔF map of **1** revealed the presence of two crystallographically independent molecules of methanol, whereas a water molecule was detected in the lattice of **2**. Hydrogen atoms were placed at calculated positions; those of lattice water molecules were located from the Fourier map and refined with constrained O–H distances of 0.85 Å. All the calculations were performed using the WinGX System, version 1.80.05.[78] Crystal data and details of refinements for all the complexes are given in Table 7.

CCDC-933620 (for **1**), -937379 (for **2**), and -937380 (for **3**) contain the supplementary crystallographic data for this paper. These data can be obtained free of charge from The Cambridge Crystallographic Data Centre via www.ccdc.cam.ac.uk/data_request/cif.

Supporting Information (see footnote on the first page of this article): X-ray crystallographic data for complexes **1**, **2**, and **3**; FTIR spectra, electronic spectra, conductivity data, and ^{1}H NMR spectra of ligands (HL^1 to HL^3).

Acknowledgments

The authors wish to thank the Council of Scientific and Industrial Research (CSIR), New Delhi [project number 01(2464)/11/EMR-II dated 16-05-2011, to D. D. and project number 09/028(0766)/2010-EMR-I dated 22/02/2010, to S. D.] for financial support. The authors also thank the Department of Science and Technology (DST), New Delhi for use of the single-crystal diffractometer facility at the Department of Chemistry, University of Calcutta, through the DST-FIST program.

[1] M. Zhao, C. Zhong, C. Stern, A. G. M. Barrett, B. M. Hoffman, *J. Am. Chem. Soc.* **2005**, *127*, 9769–9775.
[2] S. l. Triki, C. J. Gómez-García, C. J. Ruiz, E. J. Sala-Pala, *Inorg. Chem.* **2005**, *44*, 5501–5508.
[3] J. Yoon, L. M. Mirica, T. D. P. Stack, E. I. Solomon, *J. Am. Chem. Soc.* **2004**, *126*, 12586–12595.
[4] Y. Song, C. Massera, O. Roubeau, P. Gamez, A. M. M. Lanfredi, J. Reedijk, *Inorg. Chem.* **2004**, *43*, 6842–6847.
[5] K. S. Banu, T. Chattopadhyay, A. Banerjee, S. Bhattacharya, E. Suresh, M. Nethaji, E. Zangrando, D. Das, *Inorg. Chem.* **2008**, *47*, 7083–7093.
[6] N. S. A. Rey, A. Neves, A. J. Bortoluzzi, C. T. Pich, H. N. Terenzi, *Inorg. Chem.* **2007**, *46*, 348–350.
[7] M. E. Bluhm, M. Ciesielski, H. Görls, O. Walter, M. Döring, *Inorg. Chem.* **2003**, *42*, 8878–8885.
[8] K. Dhara, S. Karan, J. Ratha, P. Roy, G. Chandra, M. Manassero, B. Mallik, P. Banerjee, *Chem. Asian J.* **2007**, *2*, 1091–1100.
[9] K. Dhara, P. Roy, J. Ratha, M. Manassero, P. Banerjee, *Polyhedron* **2007**, *26*, 4509–4517.
[10] M. Fujita, Y. J. Kwon, S. Washizu, K. Ogura, *J. Am. Chem. Soc.* **1994**, *116*, 1151–1152.
[11] M. Fujita, J. Yazaki, K. Ogura, *Tetrahedron Lett.* **1991**, *32*, 5589–5592.
[12] D. Gatteschi, R. Sessoli, J. Villain, *Molecular Nanomagnets*, Oxford University Press, Oxford, UK, **2006**.
[13] a) J. R. Friedman, M. P. Sarachik, J. Tejada, R. Ziolo, *Phys. Rev. Lett.* **1996**, *76*, 3830; b) L. Thomas, F. Lionti, R. Ballou, D. Gatteschi, R. Sessoli, B. Barbara, *Nature* **1996**, *383*, 145; c) C. Sangregorio, T. Ohm, C. Paulsen, R. Sessoli, D. Gatteschi, *Phys. Rev. Lett.* **1997**, *78*, 4645; d) W. Wernsdorfer, R. Sessoli, *Science* **1999**, *284*, 133.
[14] a) M. N. Leuenberger, D. Loss, *Nature* **2001**, *410*, 789–793; b) F. Troiani, M. Affronte, *Chem. Soc. Rev.* **2011**, *40*, 3119–3129; c) F. Meier, D. Loss, *Phys. B: Condensed Matter*, part 2, **2003**, 1140–1141.
[15] M. Mannini, F. Pineider, C. Danieli, F. Totti, L. Sorace, P. Sainctavit, M. A. Arrio, E. Otero, L. Joly, J. C. Cezar, A. Cornia, R. Sessoli, *Nature* **2010**, *468*, 417.
[16] a) L. Bogani, W. Wernsdorfer, *Nat. Mater.* **2008**, *7*, 179–186; b) R. E. P. Winpenny, *Nat. Nanotechnol.* **2013**, *8*, 159–160.
[17] a) G. Christou, D. Gatteschi, D. N. Hendrickson, R. *Sessoli*, *MRS Bull.* **2000**, *25*, 66; b) D. Gatteschi, R. Sessoli, *Angew. Chem. Int. Ed.* **2003**, *42*, 268; *Angew. Chem.* **2003**, *115*, 278.
[18] a) D. Gatteschi, L. Sorace, *J. Solid State Chem.* **2001**, *159*, 253; b) M. Nakano, H. Oshio, *Chem. Soc. Rev.* **2011**, *40*, 3239–3248.
[19] A. R. Paital, A. Wu, G. Qing, G. Aromì, J. Ribas-Ariño, D. Ray, *Inorg. Chem.* **2007**, *46*, 2947–2949.
[20] A. Banerjee, S. Sarkar, D. Chopra, E. Colacio, K. K. Rajak, *Inorg. Chem.* **2008**, *47*, 4023–4031.
[21] A. R. Paital, T. Mitra, D. Ray, W. T. Wong, J. Ribas-Ariño, J. J. Novoa, J. Ribas, G. Aromì, *Chem. Commun.* **2005**, *41*, 5172–5174.
[22] A. R. Paital, D. Mandal, X. Huang, J. Li, G. Aromì, D. Ray, *Dalton Trans.* **2009**, *8*, 1352–1362.
[23] A. R. Paital, V. Bertolasi, G. Aromì, J. Ribas-Ariño, D. Ray, *Dalton Trans.* **2008**, *7*, 861–864.
[24] A. R. Paital, C. S. Hong, H. C. Kim, D. Ray, *Eur. J. Inorg. Chem.* **2007**, *12*, 1644–1653.
[25] P. K. Nanda, G. Aromì, D. Ray, *Chem. Commun.* **2006**, *30*, 3181–3183.
[26] A. R. Paital, P. K. Nanda, S. Das, G. Aromì, D. Ray, *Inorg. Chem.* **2006**, *45*, 505–507.
[27] P. K. Nanda, G. Aromì, D. Ray, *Inorg. Chem.* **2006**, *45*, 3143–3145.
[28] D. E. Fenton, H. Okawa, *Chem. Ber./Recl.* **1997**, *130*, 433–442.
[29] H. Adams, S. Clunas, D. E. Fenton, S. E. Spey, *J. Chem. Soc., Dalton Trans.* **2002**, *3*, 441–448.
[30] H. Adams, D. E. Fenton, S. R. Haque, S. L. Heath, M. Ohba, H. Okawa, S. E. Spey, *J. Chem. Soc., Dalton Trans.* **2000**, *12*, 1849–1856.
[31] T. Koga, H. Furutachi, T. Nakamura, N. Fukita, M. Ohba, K. Takahashi, H. Okawa, *Inorg. Chem.* **1998**, *37*, 989–996.
[32] S. Uozumi, H. Furutachi, M. Ohba, H. Okawa, D. E. Fenton, K. Shindo, S. Murata, D. J. Kitko, *Inorg. Chem.* **1998**, *37*, 6281–6287.
[33] J. Reim, R. Werner, W. Haase, B. Krebs, *Chem. Eur. J.* **1998**, *4*, 289–298.
[34] P. Roy, M. Nandi, M. Manassero, M. Ricco, M. Mazzani, A. Bhaumik, P. Banerjee, *Dalton Trans.* **2009**, *43*, 9543–9554.
[35] M. Sarkar, R. Clérac, C. Mathonière, N. G. R. Hearns, V. Bertolasi, D. Ray, *Inorg. Chem.* **2011**, *50*, 3922–3933.
[36] M. Bera, W. T. Wong, G. Aromi, J. Ribas, D. Ray, *Inorg. Chem.* **2004**, *43*, 4787–4789.
[37] H. Adams, S. Clunas, D. E. Fenton, D. N. Towers, *J. Chem. Soc., Dalton Trans.* **2002**, *21*, 3933–3935.
[38] H. Adams, D. E. Fenton, P. McHugh, *Inorg. Chem. Commun.* **2004**, *7*, 147–150.
[39] X.-N. Cheng, W. Xue, J.-H. Huang, X.-M. Chen, *Dalton Trans.* **2009**, *29*, 5701–5707.
[40] A. K. Ghosh, D. Ghoshal, E. Zangrando, J. Ribas, N. Ray Chaudhuri, *Inorg. Chem.* **2007**, *46*, 3057–3071.
[41] C. Biswas, P. Mukherjee, M. G. B. Drew, C. J. Gómez-García, J. M. Clemente-Juan, A. Ghosh, *Inorg. Chem.* **2007**, *46*, 10771–10780.
[42] E. Colacio, J. M. Domínguez-Vera, M. Ghazi, R. Kivekäs, M. Klinga, J. M. Moreno, *Eur. J. Inorg. Chem.* **1999**, *3*, 441–445.
[43] L. J. Murray, M. Dinca, J. R. Long, *Chem. Soc. Rev.* **2009**, *38*, 1294–1314.
[44] J.-R. Li, R. J. Kuppler, H.-C. Zhou, *Chem. Soc. Rev.* **2009**, *38*, 1477–1504.
[45] M. P. Suh, Y. E. Cheon, E. Y. Lee, *Coord. Chem. Rev.* **2008**, *252*, 1007–1026.
[46] M. Kawano, M. Fujita, *Coord. Chem. Rev.* **2007**, *251*, 2592–2605.

[47] S. Uchida, N. Mizuno, *Coord. Chem. Rev.* **2007**, *251*, 2537–2546.
[48] M. Kurmoo, *Chem. Soc. Rev.* **2009**, *38*, 1353–1379.
[49] G. Aromí, E. K. Brechin, *Struct. Bonding (Berlin)* **2006**, *122*, 1.
[50] M. Mikuriya, D. Yoshioka, M. Handa, *Coord. Chem. Rev.* **2006**, *250*, 2194–2211.
[51] Z. Wang, G. Chen, K. Ding, *Chem. Rev.* **2009**, *109*, 322–359.
[52] L. Ma, C. Abney, W. Lin, *Chem. Soc. Rev.* **2009**, *38*, 1248–1256.
[53] J. Lee, O. K. Farha, J. Roberts, K. A. Scheidt, S. T. Nguyen, J. T. Hupp, *Chem. Soc. Rev.* **2009**, *38*, 1450–1459.
[54] T. Uemura, N. Yanai, S. Kitagawa, *Chem. Soc. Rev.* **2009**, *38*, 1228–1236.
[55] B. Kesanli, W. Lin, *Coord. Chem. Rev.* **2003**, *246*, 305–326.
[56] O. R. Evans, W. Lin, *Acc. Chem. Res.* **2002**, *35*, 511–522.
[57] M. D. Allendorf, C. A. Bauer, R. K. Bhakta, R. J. T. Houk, *Chem. Soc. Rev.* **2009**, *38*, 1330–1352.
[58] C. M. G. Dos Santos, A. J. Harte, S. J. Quinn, T. Gunnlaugsson, *Coord. Chem. Rev.* **2008**, *252*, 2512–2527.
[59] R. R. Gagne, C. L. Spiro, T. J. Smith, C. A. Hamann, W. R. Thies, A. D. Shiemke, *J. Am. Chem. Soc.* **1981**, *103*, 4073–4081.
[60] D. Das, A. Guha, S. Das, P. Chakraborty, T. K. Mondal, S. Goswami, E. Zangrando, *Inorg. Chem. Commun.* **2012**, *23*, 113–116.
[61] L. Pardi, D. Gatteschi, *Gazz. Chim. Ital.* **1993**, *123*, 231.
[62] N. F. Chilton, R. P. Anderson, L. D. Turner, A. Soncini, K. S. Murray, *J. Comput. Chem.* **2013**, *34*, 1164–1175.
[63] G. Rogez, J.-N. Rebilly, A.-L. Barra, L. Sorace, G. Blondin, N. Kirchner, M. Duran, J. van Slageren, S. Parsons, L. Ricard, A. Marvilliers, T. Mallah, *Angew. Chem. Int. Ed.* **2005**, *44*, 1876–1879; *Angew. Chem.* **2005**, *117*, 1910.
[64] B. Bleaney, K. D. Bowers, *Proc. R. Soc. London, Ser. A* **1952**, *214*, 451–465.
[65] T. Peristeraki, M. Samios, M. Siczek, T. Lis, C. J. Milios, *Inorg. Chem.* **2011**, *50*, 5175–5185.
[66] T. K. Paine, E. Rentschler, T. Weyhermüller, P. Chaudhuri, *Eur. J. Inorg. Chem.* **2003**, *17*, 3167–3178.
[67] R. Biswas, S. Mukherjee, P. Kar, A. Ghosh, *Inorg. Chem.* **2012**, *51*, 8150–8160.
[68] M. A. Palacios, A. J. Mota, J. E. Perea-Buceta, F. J. White, E. K. Brechin, E. Colacio, *Inorg. Chem.* **2010**, *49*, 10156–10165.
[69] G. Aromí, A. R. Bell, M. Helliwell, J. Raftery, S. J. Teat, G. A. Timco, O. Roubeau, R. E. P. Winpenny, *Chem. Eur. J.* **2003**, *9*, 3024–3032.
[70] L. Chen, S. R. Breeze, R. J. Rousseau, S. Wang, L. K. Thompson, *Inorg. Chem.* **1995**, *34*, 454–465.
[71] P. Mukherjee, M. G. B. Drew, C. J. Gómez-García, A. Ghosh, *Inorg. Chem.* **2009**, *48*, 5848–5860.
[72] P. Seppälä, E. Colacio, A. J. Mota, R. Sillanpää, *Inorg. Chem.* **2013**, *52*, 11092–11109.
[73] B. A. Breeze, M. Shanmugam, F. Tuna, R. E. P. Winpenny, *Chem. Commun.* **2007**, *48*, 5185–5187.
[74] M. Sarkar, R. Clérac, C. Mathonière, N. G. R. Hearns, V. Bertolasi, D. Ray, *Inorg. Chem.* **2010**, *49*, 6575–6585.
[75] *SMART, SAINT*, Software Reference Manual, Bruker AXS Inc., Madison, WI, **2000**.
[76] In *SHELXL-97*, *Programs for Crystal Structure Analysis*, release 97–2, G. M. Sheldrick, University of Göttingen, Germany, **1998**.
[77] L. J. Farrugia, *J. Appl. Crystallogr.* **1999**, *32*, 837–838.
[78] *WinGX System*, v. 1.80.05, L. Farrugia, University of Glasgow, UK.

Received: December 17, 2013
Published Online: May 8, 2014

